energies

MDPI

Article

Comparative Thermal and Demagnetization Analysis of the PM Machines with Neodymium and Ferrite Magnets

Oleksandr Dobzhanskyi [1,*], Viktor Grebenikov [2], Rupert Gouws [3], Rostyslav Gamaliia [2] and Eklas Hossain [4]

[1] Department of Natural Sciences, Engineering, and Technology, Point Park University, Pittsburgh, PA 15222, USA
[2] Institute of Electrodynamics, National Academy of Sciences of Ukraine, Pr. Peremohy, 56, 03057 Kyiv, Ukraine; elm1153@gmail.com (V.G.); rgamaleya@gmail.com (R.G.)
[3] School of Electrical, Electronic and Computer Engineering, North-West University, Potchefstroom 2520, South Africa; rupert.gouws@nwu.ac.za
[4] Department of Electrical Engineering and Renewable Energy, Oregon Institute of Technology, Klamath Falls, OR 97601, USA; eklas.hossain@oit.edu
* Correspondence: odobz@pointpark.edu; Tel.: +1-412-667-2943

Abstract: This paper provides computer analysis and experiential investigation of the permanent magnet machines with neodymium and ferrite permanent magnets to discuss the feasibility of utilizing induction machines-oriented equipment for PM machine production. For this purpose, the machines are obtained by replacing the squirrel-cage rotor of the induction motor with the flux-focusing (tangential) and surface-mounted (radial) permanent magnet rotors. Electromechanical parameters of the machines as electromagnetic torque and output power are discussed and compared. The temperatures of the neodymium and ferrite magnets are also calculated at rated current, and short circuit scenarios and the performance of two different cooling systems in minimizing the temperature effect on the machines are investigated. Furthermore, the demagnetization of permanent magnets at various load conditions is also studied. Finally, the results of the computer modeling are validated by the physical prototypes of the machines. The characteristics of the electrical machines under study were calculated using the Simcenter MagNet and Simcenter MotorSolve software packages.

Keywords: demagnetization; liquid cooling; permanent magnet; torque density

Citation: Dobzhanskyi, O.; Grebenikov, V.; Gouws, R.; Gamaliia, R.; Hossain, E. Comparative Thermal and Demagnetization Analysis of the PM Machines with Neodymium and Ferrite Magnets. *Energies* **2022**, *15*, 4484. https://doi.org/10.3390/en15124484

Academic Editor: Anibal De Almeida

Received: 19 May 2022
Accepted: 17 June 2022
Published: 20 June 2022

1. Introduction

A few decades ago, when permanent magnet (PM) technology was still developing, induction machines (IMs) dominated in the industry. However, the current progress of PM machines has led to the achievement of higher performance, improved efficiency, better reliability, higher power density, superior power factor, and synchronous operation, among many others [1]. Understandably, the scale has tipped in favor of permanent magnet machines. Therefore, the industries that initially invested in induction motors are now faced with a dilemma as reinvesting into the new assembly lines of PM machines and retiring existing IM-oriented equipment is a costly and time-consuming process with a detrimental environmental impact. Therefore, the industries attempt a different approach, where the existing IM-oriented equipment is utilized to produce PM machines. Previously, the thermal analysis of permanent magnet machines has been discussed in a significant number of papers [2–4]. The torque and efficiency calculation depending on the harmonic loss has been discussed in [5]. Performance comparisons of the PMs under different temperatures have been carried out in [6]. Different cooling strategies have been proposed for various designs of these machines involving liquid and forced-air cooling [7–9]. Reliability and the application of the cooling systems has been studied in [10,11]. Comparison between different demagnetization models of permanent magnets has been discussed in [12].

PM machine demagnetization characteristics and analysis has been discussed in [13–17]. Application and the response of the machine for high current has been discussed in [18,19]. Different analysis on the PM machines has been carried out in [20].

Since the cost of rare-earth magnets is constantly increasing, there is a significant interest in machines with ferrite magnets. Therefore, the importance of this research is outlined by the necessity to design rare-earth-free machines, which could compete with their rare-earth counterparts in power density and efficiency. This paper provides an insightful comparison of the PM machines with rare-earth and ferrite PMs to reach this goal. In addition, the machines are compared in terms of output power, electromagnetic torque temperature distribution, and demagnetization of permanent magnets at various load conditions.

This paper demonstrates how the conventional squirrel cage induction motor can be converted into an efficient PM motor at a low cost. For this reason, the squirrel cage rotor of the induction motor is replaced with a permanent magnet rotor. In order to investigate the influence of the rotor configuration on the machine's characteristics, two rotors: (a) with tangential PMs and (b) with radial PMs are studied. Furthermore, 3D Finite Element Method (FEM) analysis is applied to investigate the electromagnetic and temperature phenomena in the machines. Finally, specific attention is paid to the demagnetization of permanent magnets during short-circuit scenarios when the current is 6.5–15 times higher than the rated current.

The rest of the paper is organized as follows. Section 2 contains the performance analysis of the of the PM machines with rare earth and ferrite magnets; Section 3 elaborately discusses the temperature analysis of the tangential and radial machines with rare earth and ferrite magnets. Demagnetization analysis of the magnets at high load current is discussed in Section 4. Next, Section 5 provides experimental validation for the obtained simulation results. Finally, Section 6 concludes the paper

2. Performance Analysis of the Machines with Rare-Earth and Ferrite PMs

In order to study the possibility of replacing the rare-earth magnets with ferrite magnets in the PM machines, the rotors with rare-earth (N42) and ferrite (C10) PMs are discussed. As known, neodymium magnets (N42) demonstrate operational stability up to 80 °C. This temperature can be higher for other rare-earth magnets such as N45SH, where the temperature stability reaches 150 °C. However, N45SH PMs have higher costs compared to N42 magnets and are not widely available on the market. Therefore, this study will be focused on N42 magnets whose residual flux density is 1.2 T.

As for the ferrite magnets (C10), the working temperature of these magnets is higher than that of the neodymium ones and can reach up to 300 °C. The residual flux density of these magnets is, however, around three times lower than that of the N42 PMs and equals 0.4 T. Both tangential and radial machines, which are discussed further, employ a stator of the conventional squirrel-cage motor, with characteristics enclosed in Table 1.

The tangential machine with internal PMs is depicted in Figure 1a. The machine is analyzed using Simcenter MagNet® (version number 2022.1, Siemens Industry Software Inc., Plano, TX, USA) and MotorSolve® (version number 2022.1, Siemens Industry Software Inc., Plano, TX, USA) software. The two way analysis between the electromagnetic and mechanical solver is enabled to calculate temperature by solving conjugate problems. The magnetic flux densities in this machine's stator and rotor core for N42 and C10 PMs are illustrated in Figure 1b,c respectively. The magnetic flux density values in the machine with neodymium PMs are as follows: 1.7 T—in the stator core, 2.1 T—in the stator teeth, and 1.5 T—in the rotor core. The same values in the machine with ferrite magnets (Figure 1c) are: stator core—0.9 T, stator teeth—1.6 T, and rotor core is 0.8 T. The machine with radial (surface-mounted) PMs is depicted in Figure 2a, and the magnetic flux distribution of this machine for N42 and C10 magnets is plotted in Figure 2a,b. The magnetic flux density values in the machine with N42 PMs (Figure 2b) are 1.4 T—stator core, 2 T—stator, and 1 T—rotor core. The values in the machine with ferrite magnets are (Figure 2c): stator core—0.6 T, stator teeth—1 T, and stator core—0.5 T. The coercivity of the magnets at 300 and 400 K multiplied by the relative permeability is provided Table 1.

Table 1. Basic parameters of the conventional squirrel-cage induction motor.

Parameter	Value
Number of poles	4
Number of slots	36
Diameter (Outer)	130 mm
Diameter (Inner)	89 mm
Air-gap	1 mm
Terminal voltage *Vt*	380 V
Rated current *Ia*	1.2 A
Ratedoutput power, *P*	550 W
Rated speed, n	650 rpm
Efficiency	65%
Power factor	0.6
Phase resistance	90 Ohms
Filling factor	0.6
Thermal coercivity of the N42 at:	
300 K	1.23 T
400 K	0.01 T
Thermal coercivity of the C10 at:	
300 K	0.35
400 K	0.29
Electrical conductivity of the N4	0.667×10^6 S/m
Electrical conductivity of the C10	Non conductive

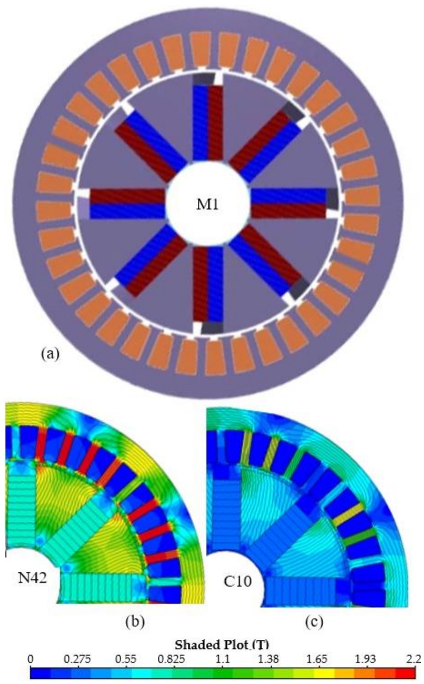

Figure 1. Tangential machine: (**a**) general view, (**b**) magnetic flux density in the stator and rotor core of N42 PM machine, (**c**) magnetic flux density distribution in the stator and rotor core of C10 PM machines.

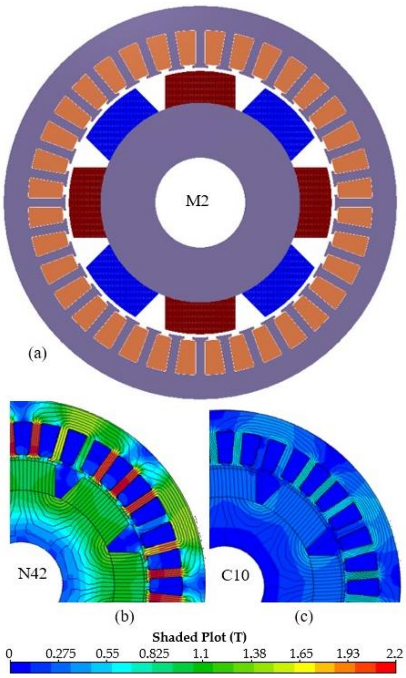

Figure 2. Radial machine: (**a**) general view, (**b**) magnetic flux density in the stator and rotor core of N42 PM machine, (**c**) magnetic flux density distribution in the stator and rotor core of C10 PM machines.

The magnetic flux in the stator teeth interacting with the current in the stator winding produces electromagnetic torque in the machine. A product of the electromagnetic torque and speed of the rotor results in output power on the machine's shaft. The output power and the electromagnetic torque characteristics for tangential and radial machines with rare-earth (N42) and ferrite (C10) PMs are compared in Figure 3. In this comparison, the number of turns in both machines is N = 90.

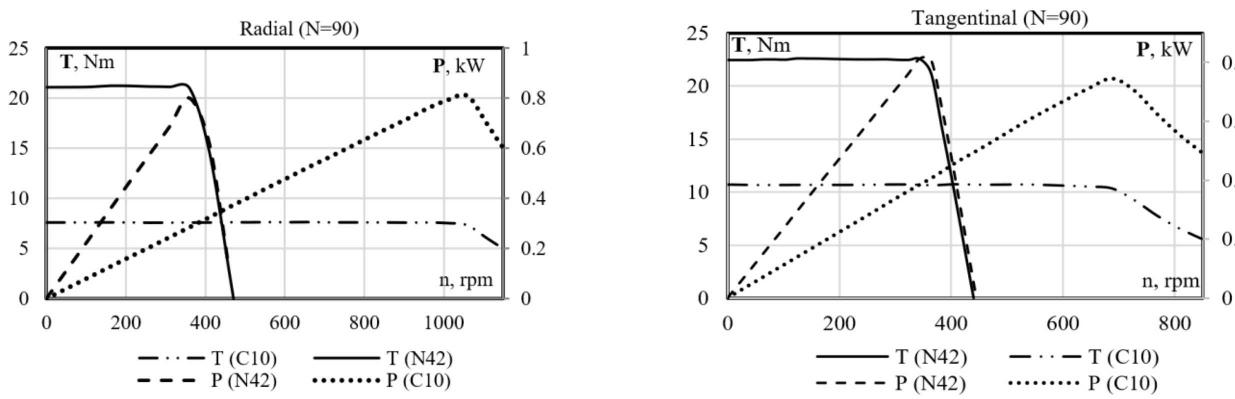

(**a**) (**b**)

Figure 3. Electromechanical characteristics of the tangential and radial machines with N42 and C10 PMs for N = 90 turns. Here, the *X*-axis defines the speed of the machines and the *Y*-axis shows the torque and output power.

The output power and electromagnetic torque of the tangential machine with N42 PMs decrease rapidly when the machine reaches the speed of 350 rpm (Figure 3a). On the other hand, the same tendency is observed for the machine with ferrite magnets, but at a speed of 690 rpm.

The maximum torque of the tangential machine with N42 PMs is two times higher than that of the machine with ferrite magnets. The higher value of the magnetic flux density in the stator teeth of the machine with rare-earth magnets explains this phenomenon. The maximum output power of the tangential machine with N42 PMs equals 0.8 kW at the speed of 380 rpm, and for the machine with ferrite magnets, 0.76 kW at the speed of 690 rpm

On the other hand, the maximum output power of the radial machine with N42 PMs (Figure 2b) is the same as that of the tangential machine with rare-earth magnets: 0.8 kW at a speed of 380 rpm. The same power is observed in the machine with C10 PMs, however, at a speed of 1060 rpm. The maximum torque (T) of the tangential and radial machines with N42 PMs (Figure 3a,b) is also similar: 23 Nm for the tangential; and 22 Nm for the radial. This torque is constant for both machines at the speed range of 0–380 rpm. For the machines with ferrite magnets, the torque is 10.5 Nm for the tangential; and 7.8 Nm—for the radial machine. Additionally, the constant torque speed range for these machines is as follows: 0–690 rpm for the tangential machine; and 0–1100 rpm for the machine with radial PMs. When the number of turns in both machines is decreased to N = 20, the torque and power characteristics change, as portrayed in Figure 4. Now the maximum output power of the tangential and radial machines with N42 PMs is five times higher than the machines with N = 90 turns (Figure 4a,b).

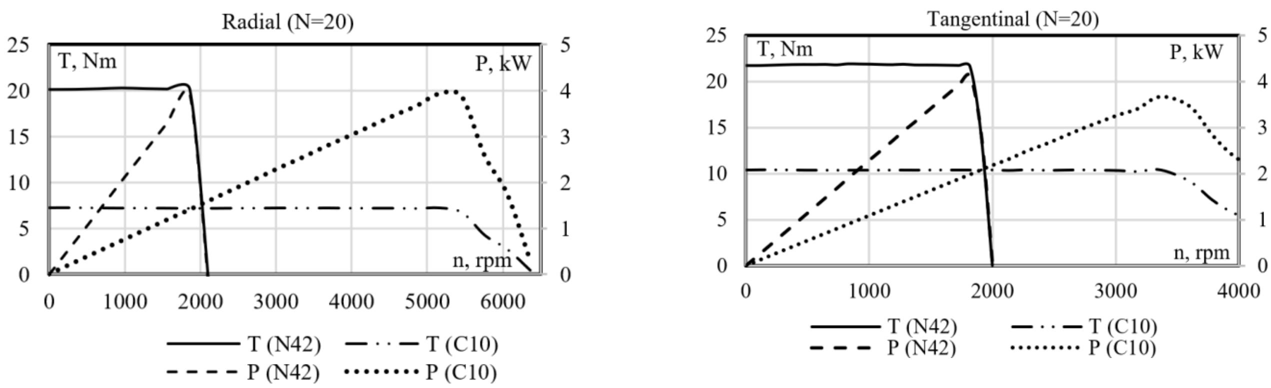

(**a**) (**b**)

Figure 4. Electromechanical characteristics of the tangential and radial machines with N42 and C10 PMs for N = 20 turns. Here, the *X*-axis defines the speed of the machines and the *Y*-axis shows the torque and output power.

The same is observed in the machines with C10 magnets. The output power (P) increases due to the decrease of the synchronous reactance by the lower number of turns. Moreover, the speed span at which the machines operate with constant torque has also increased. For the machines with N42 PMs, this range has become 0–1950 rpm. Furthermore, for the machine with C10 magnets, the constant torque operation is observed at 0–3500 rpm—for the tangential and 0–5250 for the radial. The power factor of the machines is 0.95 as the resistive load is used for the analysis.

Further decrease in the number of turns results in additional power rise of the machines and wider constant torque range-characteristics of the machine when the number of turns N = 10 are illustrated in Figure 5.

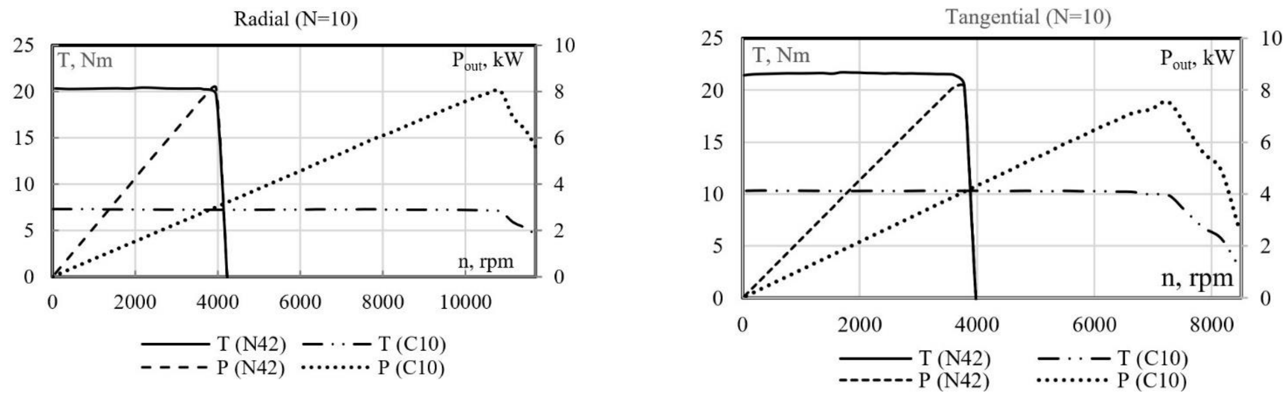

(**a**) (**b**)

Figure 5. Electromechanical characteristics of the tangential and radial machines with N42 and C10 PMs for N = 10 turns. Here, the *X*-axis defines the speed of the machines and the *Y*-axis shows the torque and output power.

The maximum power of the tangential and radial machines with N42 magnets is now increased to 8.05 kW. The power of the machines with ferrite magnets is as follows: 7.7 kW—for the tangential and 8 kW for the radial machine. Even though the maximum powers of machines with N42 and C10 magnets are similar, the speed corresponding to these powers is different. To reach 7.7 kW, the tangential machine with ferrite magnets needs to develop a speed of 7050 rpm. The machine with N42 magnets—3850 rpm. As soon as such speed is reached, the output power of the tangential machine starts to decrease rapidly due to the high eddy loss. In the case of the machines with ferrite magnets, these losses are lower because of the lower residual flux of the ferrite magnets.

To conclude, the tangential and radial machines with N = 10 turns develop higher maximum power and operate with a broader range of constant electromagnetic torque than those with N = 90 and N = 20 turns. Therefore, the machines with N = 10 turns will be considered for further analysis. The output power of the tangential machine with N42 PMs and N = 10 turns at the speed of 650 rpm (Figure 5) is 5.5 times higher than the power of the conventional squirrel-cage rotor machine (Table 1) at the same speed. To evaluate the efficiency of the radial and tangential machines with N = 10 turns, the hysteresis, eddy current, and ohmic losses in all the elements of the machine such as stator core, rotor, magnets, stator teeth, and the winding are calculated using 3D FEM. The results of the simulations are presented in Table 2.

Table 2. Power loss in the tangential and radial machines with N = 10 turns.

Parameter	Tangencial (N42)	Tangencial (C10)	Radial (N42)	Radial (C10)
n, rpm	3000	3000	3000	3000
Torque (N·m)	21.8	9.2	19.9	6.2
Efficiency (%)	96.5	91.8	96.2	90.07
Loss—Total (W)	301.5	259.5	273.5	215.9
Loss—Winding (W)	173.4	227.8	177.0	204.7
Loss—Stator back iron hysteresis (W)	45.68	9.83	36.00	4.18
Loss—Stator back iron eddy current (W)	21.08	2.83	12.72	0.97
Loss—Stator teeth hysteresis (W)	32.38	13.81	27.15	4.45
Loss—Stator teeth eddy current (W)	24.98	4.52	15.12	1.40
Loss—Rotor back iron hysteresis (W)	0.96	0.41	0.010	0.011
Loss—Rotor back iron eddy current (W)	1.04	0.35	0.002	0.003
Loss—Magnets eddy current (W)	2.00	0	0.005	0

Both tangential and radial machines with N42 magnets exhibit higher power losses than the same machines with C10 PMs due to the higher residual flux of the rare-earth magnets. These power losses of the machines cause a rise in the temperature in the elements of the machine. Therefore, a thorough temperature analysis is necessary to investigate the effect of temperature on the operational characteristics of the machines.

3. Thermal Analysis of the Machines with Rare-Earth and Ferrite PMs

The temperature analysis of the machines (including winding, PMs, shaft, bearings, stator, and rotor core) is carried out using Simcentr MotorSolve. The machines are operated continuously until the components of the machines reach the steady-state temperature. Then, two cooling systems—air-forced and liquid, are applied to evaluate the more suitable system for the presented machines. In order to perform a conjugate heat transfer simulation in the software, appropriate boundary conditions were set up. Mainly those are: periodic boundary since the model was cut by sectors, external and internal boundaries. The heat transfer within the boundaries is completed either by convection or conduction. Mesh adaption and verification was completed to obtain an accurate solution. When the thermal model was set up, the power losses of the electromagnetic solver were mapped to the thermal solver.

The air-forced cooling system is characterized by the air moving alongside the machine's stator. The system is designed with the following initial parameters:

- The machine is oriented horizontally.
- The speed of the coolant flow = 2 m/s.
- The initial temperature of the machine is T = 20 °C.

With the help of parametric analysis, the temperature of the PMs is calculated for machines with a varying number of turns. In this analysis, the machines evolve the air-forced cooling. The temperature curves of the permanent magnets in the machines with N = 90, 20, and 10 turns are plotted in Figure 6a,b. Here, solid lines indicate the curves for the neodymium magnets (N42), and the dotted lines illustrate the characteristics of the machine with ferrite magnets (C10).

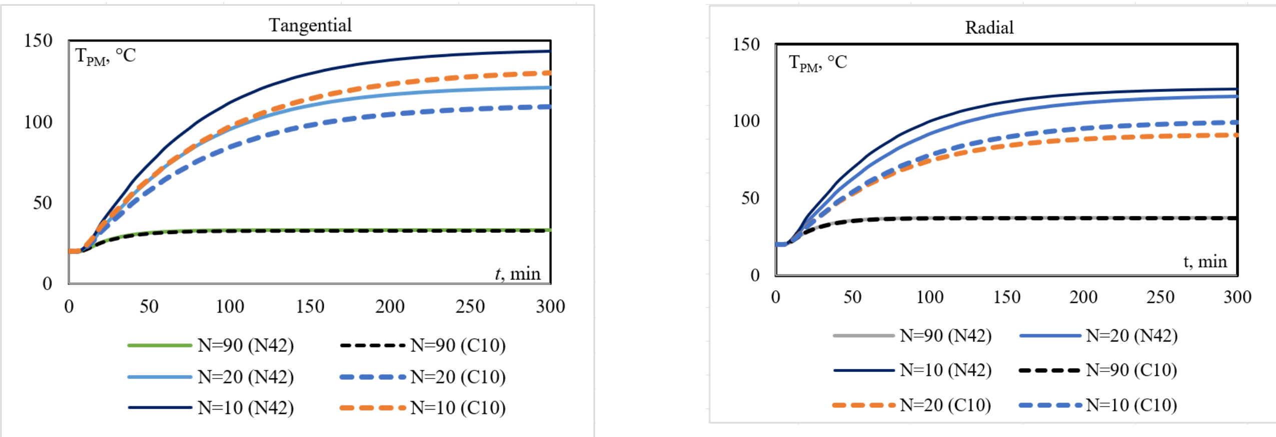

(**a**) (**b**)

Figure 6. Temperature characteristics of the PMs in the tangential and radial machines with various numbers of turns at air-forced cooling. Here, the *X*-axis defines the time and the *Y*-axis shows the temperature of the machines.

The results show that the temperature of the C10 magnets in the machine with tangential PMs does not exceed 100 °C (Figure 6a), and the temperature of the C10 magnets in the radial machine is 130 °C (Figure 6b).

Therefore, since the maximum working temperature of the ferrite magnets is 130 °C, the proposed air-forced cooling system can satisfy the operating conditions of these PMs. The temperature of the N42 magnets for both tangential (Figure 6a) and radial (Figure 6b) machines is higher than the working temperature of these magnets (80 °C). Therefore, the proposed air-cooling system is not sufficient for the proposed machines with N42 PMs, and so, the liquid cooling for the machines with N42 magnets is explored next.

The discussed liquid cooling system is placed along the rotor shaft and composed of the water channels equally distributed in the inner part of the machine. The water moves inside these channels with the help of the circulating pump. Thus, the heat generated in the machine's elements is transferred to the water. The initial data for the liquid cooling system are as follows:

- The number of cooling channels is 100.
- The shape of the cooling channels is circular.
- The diameter of the cooling channels is 3 mm.
- The initial water temperature is 20 °C.

The cooling efficiency of the liquid system depends on the circulating pump. Therefore, the system was analyzed for various water flow values ranging from 0 to 4 L/minute to find a suitable pump for the design. The performance of the cooling system for different flow rates is presented in Figure 7. The analysis was carried out for the number of turns N = 10 and rated current density J = 8.5 A/mm^2.

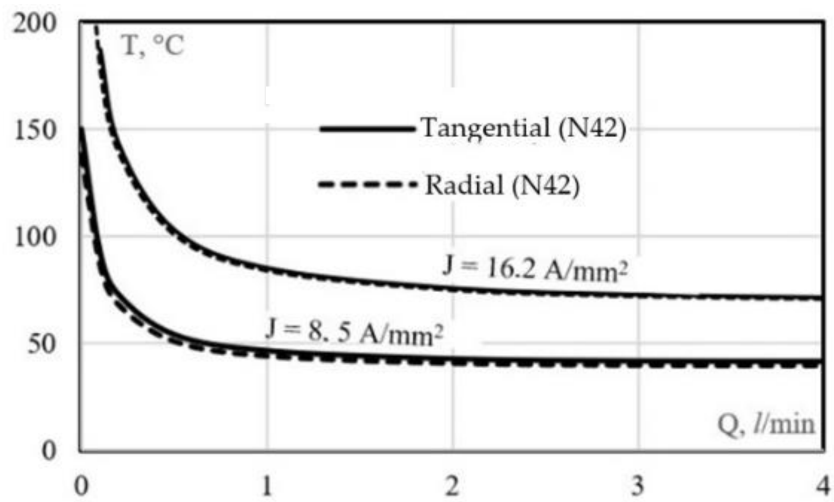

Figure 7. Temperatures of the neodymium magnets (N42) in the tangential and radial machines at various water flow rate of the liquid cooling system. Here, the *X*-axis defines the flow rate of the system and the *Y*-axis shows the temperature of the machines.

Additional calculation of the temperature in the machines is provided for the current density J = 16.2 A/mm^2. The graphs demonstrate, when the circulation pump performs at a water flow of 2 L/min, even for an increase in flow rate, the temperature of the magnets is unchanged. Therefore, the value Q = 2 L/min can be taken as optimal. At such optimal pump performance, the steady-state temperature of the tangential magnets and radial PMs are 42.6 °C and 41.1 °C respectively. The thermal models of the tangential and radial machines are shown in Figure 8. For the rated current density of the machines, the temperature distribution in the machine's elements is plotted in Figure 8a,b. For the current density 1.9 times higher than that of the rated value, this field is depicted on Figure 8c,d. This analysis demonstrates that the lowest temperature is observed inside the outer casing, where the cooling channels are located. Conversely, the highest temperature is in the machines' windings and the permanent magnets. Additionally, the analysis also demonstrates that liquid cooling can maintain the temperature of the N42 PMs below the critical temperature of 80 °C. Moreover, the proposed cooling system is also found to be efficient at a winding current 1.9 times higher than the rated value.

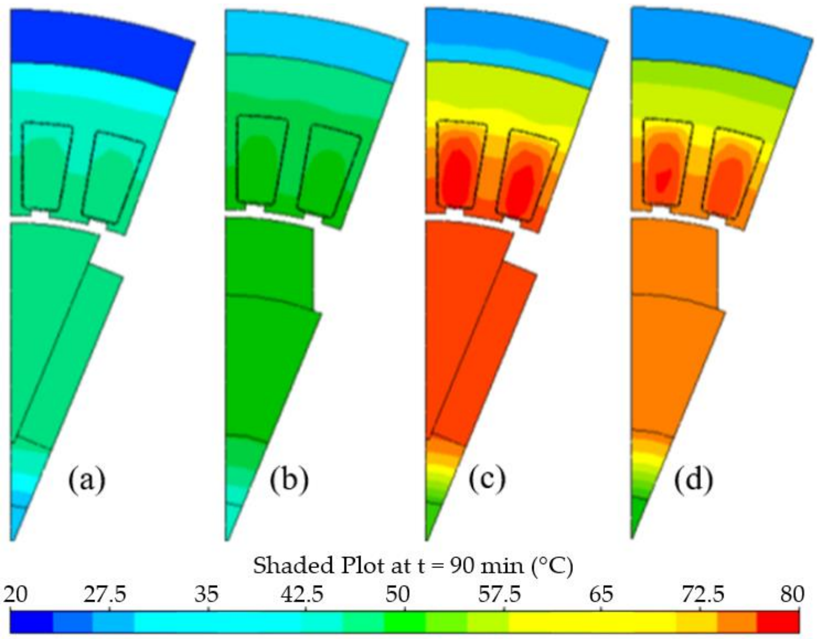

Figure 8. Thermal models of the tangential and radial machines with various current density (J) in the winding: (**a**) tangential machine with J = 8.5 A/mm^2, (**b**) radial machine with J = 8.5 A/mm^2, (**c**) tangential machine with J = 6.2 A/mm^2, (**d**) radial machine with J = 16.2 A/mm^2.

Thermal properties of the materials involved in the simulation are specified in the software before the analysis. These include thermal modifiers for the permeability and thermal coercivity of permanent magnets, and also cooper conductivity.

4. Demagnetization Analysis of the Machines at High Current Loading

In this section a demagnetization analysis of the machines with different current values is carried out in software packages Simcentr MotorSolve. With the help of this software, the breaking point of the demagnetization curve, where the curve ceases to be linear, is determined for tangential and radial machines, both of which employ the liquid cooling system discussed in the previous section.

The results of this study are presented in Figures 9 and 10. The demagnetization of the magnets is estimated with the help of the demagnetization prediction scale. The color on the magnets symbolizes the demagnetization probability. In the tangential machine (Figure 9), the neodymium magnets begin to demagnetize only when the current reaches a value ten times higher than the rated current I_n. The red-colored regions indicate this phenomenon at the edges of the PMs. The red color corresponds to a high probability (90–99%) on the prediction scale, meaning that these regions of the magnets are subject to irreversible demagnetization. At the current I = 12 × I_n, the demagnetization affects a more significant part of the magnets. Furthermore, at the current I = 15 × I_n, the red regions almost double in volume.

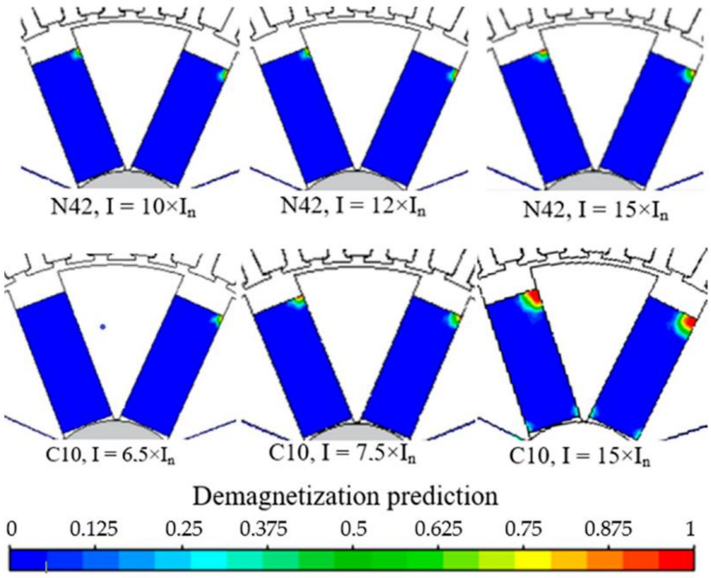

Figure 9. Results of the demagnetization analysis of N42 and C10 magnets in the tangential machine.

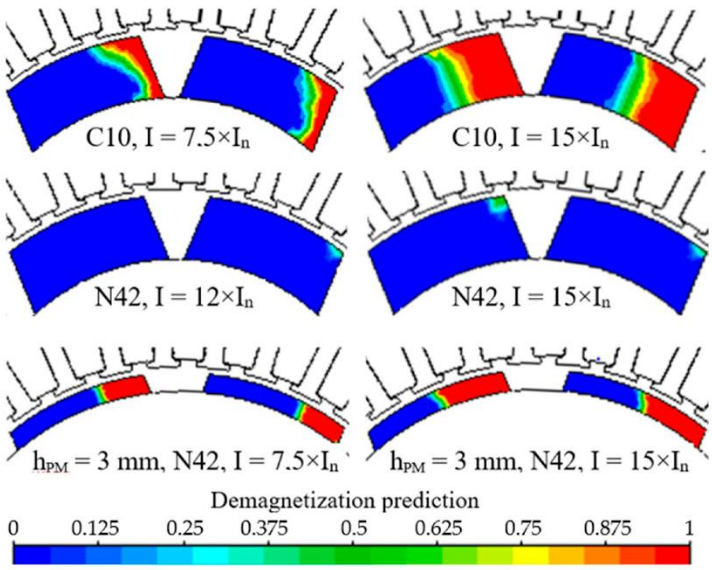

Figure 10. Results of the demagnetization analysis of N42 and C10 PMs in the radial machine.

In the ferrite magnets (C10), the demagnetization starts at the current I = 6.5 × I_n. When this current increases to I = 7.5 × I_n, a more significant part of the PMs is irreversibly demagnetized. Finally, when the stator current surges to I = 15 × I_n, the volume of the demagnetized PMs is three times higher than that of the N42 magnets at the same current. The neodymium magnets of the radial machines (Figure 10) start to demagnetize at I = 12 × I_n, and this condition exacerbates when the current increases to I = 15 × I_n.

However, the demagnetization of these magnets remains low according to the prediction scale. The opposite situation is with the ferrite magnets, which happen to demagnetize rapidly when the current exceeds the rated value. Thus, at current I = 7.5 × I_n, a considerable volume of the PMs is demagnetized, and at the current I = 15 × I_n, the machine is no longer appropriately operational.

To conclude, the demagnetization analysis demonstrates that the tangential machine, both with ferrite and neodymium magnets, is less susceptible to irreversible demagnetization compared to the radial machine. In addition, surface-mounted PMs are more exposed to the electrical field of the winding, and therefore, have lower resistance to the irreversible demagnetization under the short-circuit currents.

5. Experimental Validation of the Models with Prototype Test

The purpose of this section is to validate the computer simulations presented in the previous chapters. For this reason, the physical prototypes of the tangential and radial machines are constructed and compared performance-wise with the simulation models. The 3D FEM model of the tangential rotor and the photograph of its physical prototype are depicted in Figure 11a.

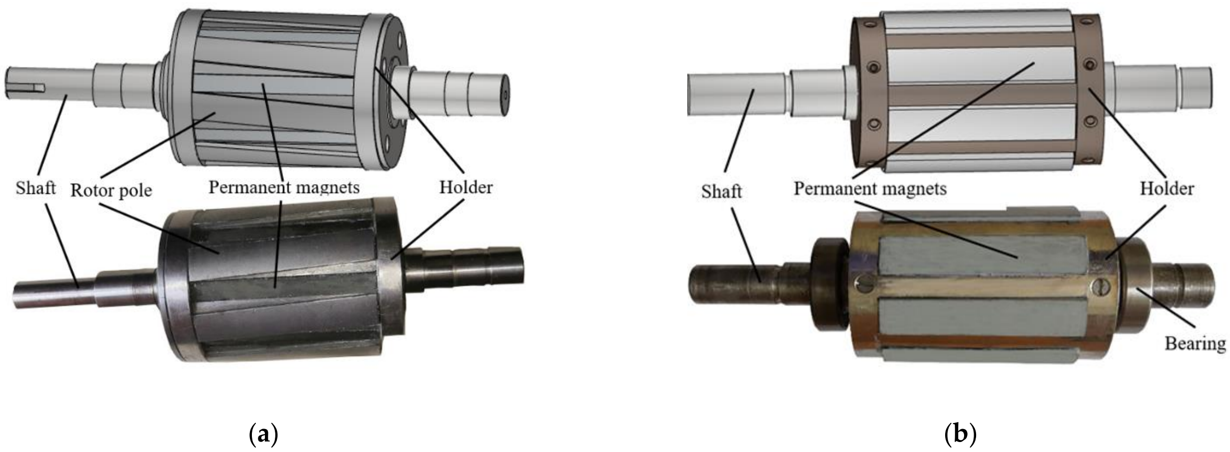

Figure 11. 3D FEM model of the PM rotor, and the photograph of its physical prototype. (**a**) Tangential rotor, (**b**) radial rotor.

The rotor of the tangential machine consists of the following elements:

(1) Shaft
(2) Rotor poles made of laminated steel
(3) PMs
(4) Non-magnetic holder

The rotor was designed to simplify the manufacturing process and, consequently, decrease the cost of the machine. In that event, four identical blocks consisting of a magnet and two rotor poles are assembled into one rotor structure and firmly attached to the rotor holder. To reduce the cogging torque, the rotor of the tangential machine is skewed by one tooth pitch, which is equal to 10°. The rotor of the machine with radial PMs is shown in Figure 11b. Similar to the rotor of the tangential machine, the radial rotor consists of the following elements:

(1) Rotor shaft
(2) Permanent magnets
(3) Non-magnetic holder

The permanent magnets are inserted into the holder and firmly attached to the holder structure. The input parameters for the simulation and physical models of the machines used to validate the paper are enclosed in Table 3.

Table 3. Parameters of the computer models used to validate the results of the study.

Parameter	Tangencial	Radial
Phase resistance, Ohm	12.5	12.5
Number of turns	90	90
Groove height, mm	12.5	12.5
Axial stator length, mm	92	100
Outer diameter of rotor, mm	87	85.5
Permanent magnet type	N42	N38
The slope of the rotor poles, deg.	10	0
Rotor core mass, kg	2.26	2.03
Rotor magnets mass, kg	1.5	1.39
Stator core mass, kg	3.44	3.71
Stator winding mass, kg	1.19	1.18
Total mass, kg	8.39	8.31
Generator total weight, kg	18	18

The experimental characteristics of the investigated machines are taken at the generator regime.

The experimental assembly used for measuring the output characteristic of the machines is shown in Figure 12. On this stand, an experimental sample of the generator 1 with the help of a drive asynchronous motor 2 is set in rotation with a given frequency from the frequency converter. The shaft of the drive motor and the generator under test are connected by means of a coupling 3.

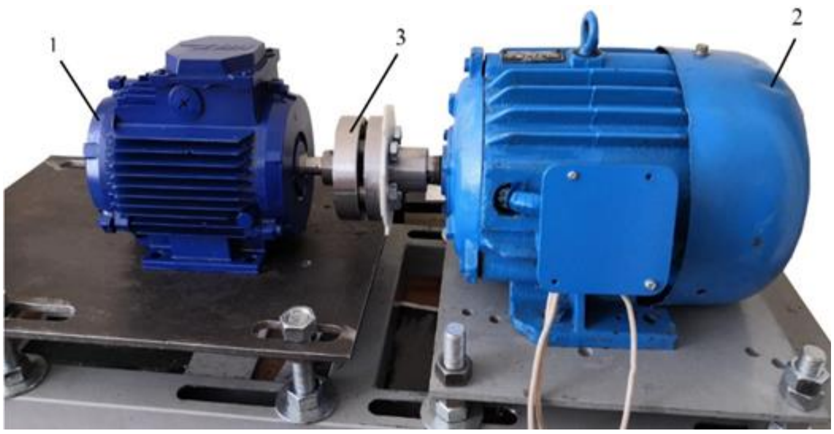

Figure 12. Experimental assembly for the investigation of tangential and radial machines in the laboratory.

Here, the tangential and radial machine 1 is driven by the asynchronous motor 2, whose speed is controlled by a frequency converter. The shafts of the drive motor and the tested machine are connected by employing clutch 3. The torque sensor is embedded between the two shafts. The infrared sensor is pointed on the shaft to measure the speed of the machine. The temperature of the winding is measured by means of two thermocouples attached to the winding surface.

During the experimental tests, the output characteristics such as terminal voltage (U_{load}) and output power (P_{load}) are measured and compared with the results of simulations models. These characteristics are illustrated in Figures 13 and 14. The characteristics of the tangential machine's terminal voltage and phase current are compared in Figure 13a, the output power with phase current for this machine is illustrated in Figure 13b, and the characteristics of the radial machine are depicted similarly in Figure 14. Analyzing the results presented in Figures 13 and 14 and Table 3, it should be noted that the power of the tangential generator is, on average, 30% higher than the power of the radial machine.

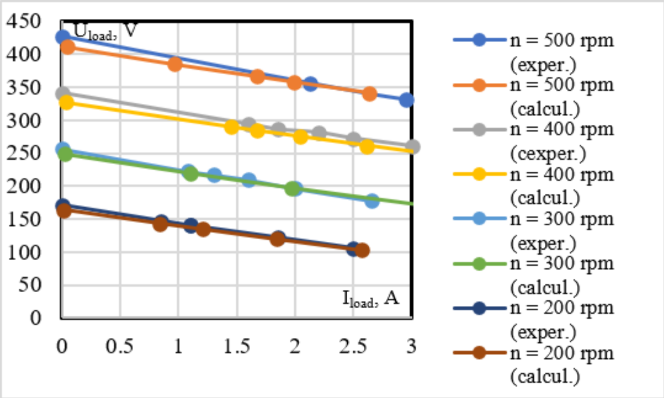

(**a**)

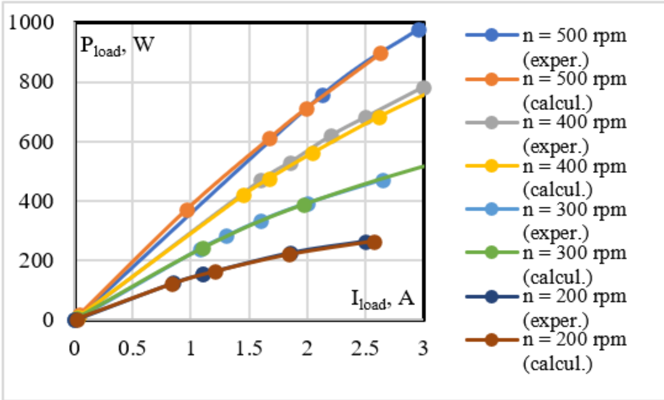

(**b**)

Figure 13. Output characteristics of the tangential machine with N42 PMs: (**a**) terminal voltage vs. load current, (**b**) output power vs. load current.

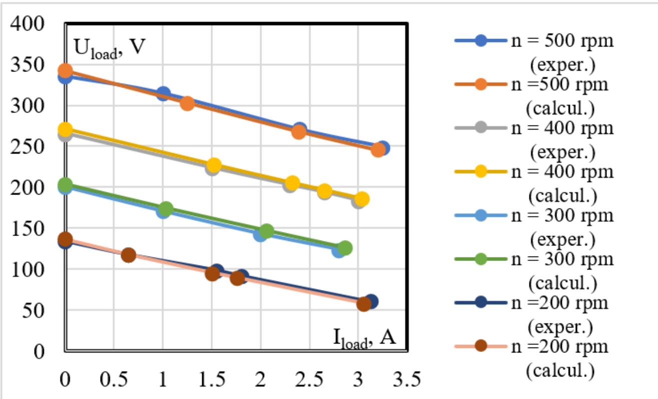

(**a**)

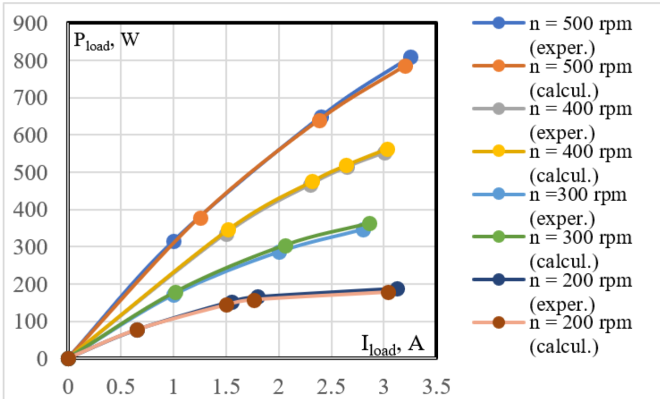

(**b**)

Figure 14. Output characteristics of the radial machine with N42 PMs: (**a**) terminal voltage vs. load current, (**b**) output power vs. load current.

The terminal voltage of both machines (Figures 13a and 14a) decrease when the load current increases. This is due to the voltage drop across the winding resistance. The experimental and calculated values of these voltages match with a negligible discrepancy of 1%. This indicates the accuracy of the 3D FEM model of the machines. The output power of the machines indicated in Figure 14a,b demonstrates the same accuracy between the experimental and calculated results. The output power of the machines at a speed n = 500 rpm continues to rise with the current loading of 3.5 A and higher, whereas the power of these machines at n = 400 rpm approaches its peak value at this load.

6. Conclusions

The study demonstrated a possibility to remodel a conventional squirrel-cage induction motor into an efficient high power density permanent magnet motor. The power of such motor can be around six times higher than that of the original induction motor. In the remodeling process, the stator of the induction motor was used, and the squirrel-cage rotor was transformed into the rotor with permanent magnets. This was done by cutting the magnet slots into the rotor core, and eliminating the cooper bars of the original squirrel-cage rotor. This process can be adopted by induction motor manufacturers who desire to produce permanent magnet machines without significant investments. Instead of manufacturing a new rotor core, for example, the conventional squeal-cage rotor is re-machined. In this case, there is no need to develop a new rotor structure which would mean using laser cut, compression rotor laminations, assembling a new bearing system etc. Therefore, this paper validates the validity and practicality of the approach of employing the equipment used for the production of IM machines for the production of the PM machines. Furthermore, it has been found that replacing the squirrel cage motor of the induction machines with permanent magnets can achieve superior performance compared to traditional induction machines. Future expansion of this work can focus on the performance of such modified machines in the EV and renewable energy applications.

Author Contributions: Conceptualization, O.D. and V.G.; methodology, review, conceptualization and research grant holder, R.G. (Rupert Gouws); editing E.H.; software and conceptualization, R.G. (Rostyslav Gamaleya). All authors have read and agreed to the published version of the manuscript.

Funding: This research is based on research/work supported in part by Eskom, South Africa (grant number: 26892278). The research findings are those of the authors and not of Eskom.

Institutional Review Board Statement: Not applicable.

Informed Consent Statement: Not applicable.

Data Availability Statement: Not applicable.

Conflicts of Interest: The authors declare no conflict of interest.

References

1. Mellor, P.D.; Roberts, D.; Turner, D. Lumped parameter thermal model for electrical machines of TEFC design. In *IEEE Proceedings B (Electric Power Applications)*; IET Digital Library: London, UK, 1991; Volume 138, pp. 205–218.
2. Lindström, J. *Thermal Model of A Permanent-Magnet Motor for A Hybrid Electric Vehicle*; Research Report; Department of Electric Power Engineering, Chalmers University of Technology: Göteborg, Sweden, 1999.
3. Vong, P.; Rodger, D. Coupled electromagnetic—Thermal modeling of electrical machines. *IEEE Trans. Magn.* **2003**, *39*, 1614–1617. [CrossRef]
4. Yamazaki, K.; Seto, Y. Torque and efficiency calculation of an interior permanent magnet motor considering harmonic iron losses of both the stator and rotor. *IEEE Trans. Magn.* **2003**, *39*, 1460–1463. [CrossRef]
5. Schiefer, M.; Doppelbauer, M. Indirect Slot Cooling for High- Power-Density Machines with Concentrated Winding. In Proceedings of the 2015 IEEE International Electric Machines & Drives Conference (IEMDC), Coeur d'Alene, ID, USA, 10–13 May 2015; pp. 1820–1825.
6. Ping, Z.; Ranran, L.; Thelin, P.; Nordlund, E.; Sadarangani, C. Research on the cooling system of a 4QT proof-of-concept machine used for HEV. *IEEE Trans. Energ. Convers.* **2008**, *23*, 61–67.
7. Nategh, S.; Huang, Z.; Krings, A.; Wallmark, O.; Leksell, M. Thermal modeling of directly cooled electric machines using lumped parameter and limited CFD analysis. *IEEE Trans. Energ. Convers.* **2013**, *28*, 979–990. [CrossRef]
8. Polikarpova, M.; Semken, S.; Pyrhönen, J. Reliability analysis of a direct-liquid cooling system of direct drive permanent magnet synchronous generator. In Proceedings of the 2013 Proceedings Annual Reliability and Maintainability Symposium (RAMS), Orlando, FL, USA, 28–31 January 2013.
9. Ridley, G. The UK's first direct-water-cooled pumped-storage generator-motor. *IEEE Electron. Power* **1982**, *28*, 678–681. [CrossRef]
10. Ruoho, S.; Dlala, D.; Arkkio, A. Comparison of demagnetization models for finite-element analysis of permanent-magnet synchronous machines. *IEEE Trans. Magn.* **2007**, *43*, 3964–3968. [CrossRef]
11. Welchko, B.; Jahns, T.; Soong, W.; Nagashima, J. IPM synchronous machine drive response to symmetrical and asymmetrical short circuit faults. *IEEE Trans. Energ. Convers.* **2003**, *18*, 291–298. [CrossRef]
12. Kang, G.; Hur, J.; Nam, H.; Hong, J.; Kim, G. Analysis of Irreversible Magnet Demagnetization in Line-Start Motors based on Finite Element Method. *IEEE Trans. Magn.* **2003**, *39*, 1488–1491. [CrossRef]
13. Choi, G.; Jahns, T. Interior permanent magnet synchronous machine rotor demagnetization characteristics under fault conditions. In Proceedings of the 2013 IEEE Energy Conversion Congress and Exposition, Denver, CO, USA, 15–19 September 2013.
14. Kimiabeigi, M.; Widmer, J.; Long, R.; Gao, Y.; Goss, J.; Martin, R.; Lisle, T.; Soler Vizan, J.; Michaelides, A.; Mecrow, B. High-Performance Low-Cost Electric Motor for Electric Vehicles Using Ferrite Magnets. *IEEE Tran. Ind. Electron.* **2016**, *63*, 113–122. [CrossRef]
15. Chiba, K.; Chino, S.; Takemoto, S.; Ogasawara, S. Fundamental Analysis of a Ferrite Permanent Magnet Axial Gap Motor with Coreless Rotor structure. *IEEJ J. Ind. Appl.* **2014**, *3*, 47–54. [CrossRef]
16. Fasil, M.; Mijatovic, N.; Jensen, B.B.; Holbøll, J. Performance Variation of Ferrite Magnet PMBLDC Motor with Temperature. *IEEE Trans. Magn.* **2015**, *51*, 1–6. [CrossRef]

17. Matsui, Y.; Shima, K.; Fukami, T.; Hanaoka, R.; Takata, S. Magnetic field analysis of a PM-assisted salient-pole synchronous generator with ferrite magnets. In *Papers of Technical Meeting on Rotating Machinery*; IEE Japan: Tokyo, Japan, 2008; Volume 13, pp. 19–24.
18. Shima, K.; Matsui, Y.; Fukami, T.; Hanaoka, R.; Takata, S. Finite element analysis of permanent-magnet-assisted salient-pole synchronous machines under load conditions. *Stud. Appl. Electromagn. Mech.* **2010**, *33*, 398.
19. Hosoi, T.; Watanabe, H.; Shima, K.; Fukami, T.; Hanaoka, R.; Takata, S. Demagnetization analysis of additional permanent magnets in salient pole synchronous machines under sudden short circuits. In Proceedings of the XIX International Conference on Electrical Machines-ICEM 2010, Rome, Italy, 6–8 September 2010.
20. Lee, J.H.; Hong, J.P. Permanent Magnet Demagnetization Characteristic Analysis of a Variable Flux Memory Motor Using Coupled Preisach Modeling and FEM. *IEEE Trans. Magn.* **2008**, *44*, 1550–1553. [CrossRef]